

Fuzzy optimal energy management for fuel cell and supercapacitor systems using neural network based driving pattern recognition

Ridong Zhang, Jili Tao, and Huiyu Zhou

Abstract— A novel adaptive energy management strategy is proposed for real time power split between fuel cells and supercapacitors in a hybrid electric vehicle in view of the fact that driving patterns greatly affect fuel economy. The driving pattern recognition (DPR) is achieved based on the features extracted from the historical velocity window with a multi-layer perceptron neural network. After the DPR has been obtained, an adaptive fuzzy energy management controller is utilized for power split according to the required power for vehicle running. In order to prolong the fuel cell lifetime whilst decreasing the hydrogen consumption, a genetic algorithm is applied to optimize critical factors such as adaptive gains and fuzzy membership function parameters for several standard driving cycles. In the proposed method, the future driving cycles are not required and the current driving pattern can be successfully recognized, demonstrating that less current fluctuations and fuel consumption can be achieved under various driving conditions. Compared with conventional energy management systems, the proposed framework can ensure the state of charge of supercapacitors within the desired limit.

Index Terms— Driving pattern recognition; Neural network classifier; Fuzzy energy management; Genetic Algorithm; FC/SC hybrid electric vehicle

I. INTRODUCTION

ENERGY crisis, environmental pollution and global warming cause fuel cells (FCs) powered vehicles to draw a lot of attention due to their high reliability and low pollutant emission [1]. However, due to slow dynamic response and limited load following capability, hydrogen starvation may occur at power fluctuations, which is impermissible for vehicles [2]. Energy storage devices, such as batteries or capacitors, are usually hybridized by a fuel cell bank as a power buffer during climbing, acceleration and braking [3][4]. Supercapacitors (SCs) have several advantages, such as long life cycle, high power density and fast charge/discharge performance [5], which is an efficient solution to satisfy large instantaneous

power requirements, absorb the feedback energy and downsize the fuel cells.

To achieve efficient power management for a hybrid electric vehicle (HEV), a variety of control strategies have been proposed, such as Haar-wavelet energy management systems [6], heuristic controllers [7], and distributed power management controllers [8], which split the energy in terms of their frequency characteristics. However, the design process is relatively complex and optimization is not considered. To further improve the performance of energy manage systems (EMSs) for HEV, optimization algorithms, such as, dynamic programming [9], genetic algorithms (GA) [10], particle swarm optimization (PSO) algorithms [11], and differential evolution (DE) [12] have been adopted. It shows that up to 30% fuel consumption was decreased over conventional vehicles [13]. Moreover, with the introduction of advanced control systems, model predictive control (MPC) [14], neural networks [15] and fuzzy logic controllers (FLCs) [16] have been widely employed to develop online and optimal energy management strategies. Among them, fuzzy energy management controllers and their variants [17][18] have become increasingly popular. To construct a fuzzy EMS, the fuzzy rule base and its membership functions should be defined in advance. The expert knowledge can be used to formulate the fuzzy rules, but there are still various fuzzy rules and membership functions to be chosen. Trials and errors as well as optimization methods are usually utilized to design a fuzzy EMS [16][19], however, the former is a time consuming experimental procedure, while most of the optimization methods only aimed at fuel consumption. Multi-objective optimization considering fuel cell lifetime and driving performance for energy management are studied continuously and has obtained promising simulation results [12][13][20], however, how to determine a fuzzy EMS including multiple objectives is still a challenge.

Driving patterns have an important impact on the fuel economy of hybrid vehicles, and the energy management systems have obtained better control performance using prior knowledge of the driving cycle [11][21]. However, the actual driving cycles are difficult to know in advance except for the traffic information provided by the global positioning systems (GPS), geographic information systems (GIS), and intelligent transport systems (ITS) [22-24]. Compared with traffic information based driving cycle identification methods, the driving information gathered from on-vehicle sensors are more applicable, convenient and reliable. Recently, k-nearest neighbor [21], fuzzy logic classifiers [25], neural networks [26],

Manuscript received August 31, 2017; revised March 29, 2018 and May 29, 2018; accepted June 26, 2018. This work was supported in part by the National Natural Science Foundation of China under Grant (61603337). H. Zhou was supported by UK EPSRC under Grant EP/N011074/1 and Royal Society-Newton Advanced Fellowship under Grant NA160342.

R. Zhang is with the Belt and Road Information Research Institute, Automation College, Hangzhou Dianzi University, Hangzhou, 310018, P.R. China (e-mail: zrd-el@163.com).

J. Tao is with Ningbo Institute of Technology, Zhejiang University, Ningbo, 315100, China (e-mail: tj1810@126.com).

H. Zhou is with Department of Informatics, University of Leicester, LE1 7RH, United Kingdom. (e-mail: hz143@leicester.ac.uk).

Euclidean distance methods [27], support vector machine [28], Hamiltonian based control optimal methods [29], and Bayesian probability estimation [30] have been utilized to recognize the driving patterns. Many researchers have worked on how to identify and classify the driving patterns, and progress has been made on how to apply this information to EMS for HEV, e.g., 1.5% improvement of fuel economy [31], 22% less fuel is consumed compared with ECMS equivalent factors of US06 [27]. The multi-layer perceptron neural network (MLP NN) classifier has been evolved to be a valuable classification tool with a significant influence on pattern recognition theory and practice [32][33], which can be adopted for driving cycle recognition. After training using the features extracted from known driving cycles, neural network classifiers can be used to identify driving patterns in real time. However, how to combine the classified information with the energy management controller without the complicated structure and heavy computation is critical for driving pattern based EMS.

In this paper, a neural network classifier based adaptive fuzzy logic energy management controller is proposed without using future driving patterns, which can be implemented in real time. Except for fuel consumption minimization, load variation minimization is considered in the objective function to prolong the fuel cell lifetime. The adaptive coefficients and the critical parameters of fuzzy rules are optimized using a genetic algorithm. The weighted sum of objectives (WSO) method in [34] is utilized to change the multiple objectives into a single objective and this time-consuming optimization process is done off-line. After optimization, the adaptive EMS is applicable in real time and easier for implementation. Online power prediction in HEV should be considered because the demand power is unknown in practice, but here the study is focusing on the optimal fuzzy management control design and the required power is obtained by an advanced vehicle simulator (ADVISOR) [35] from the congested urban roads, flowing urban roads, subway and high way conditions, which is also utilized to show the effectiveness of the proposed fuzzy energy management strategy.

The paper is organized as follows: Section 2 gives the structure of HEV powertrain, the model of the fuel cell and the supercapacitor. Section 3 details the neural network classifier, fuzzy energy management controller and GA optimization process. Section 4 conducts the applications on four typical traffics in the congested urban, flowing urban, subway and high way. Conclusions are given in Section 5.

II. SYSTEM DESCRIPTION AND MODELING

A. Powertrain structure

The structure of the powertrain for FC/SC HEV is illustrated in Fig.1, which is a set of hybrid vehicles [36]. The core of the powertrain is a hybrid of a fuel cell stack and a supercapacitor storage component.

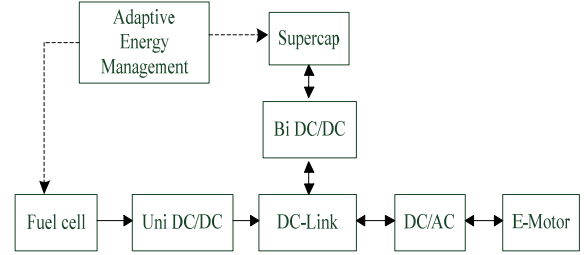


Fig.1 The structure and main components in the powertrain

The fuel cell applies the primary power and the supercapacitor provides the peak power during cold start, hard acceleration and absorbs regenerative braking energy. A 49kW alternating current (AC) permanent magnet motor is the load in the powertrain. An unidirectional DC/DC converter is connected to the FC and a bidirectional DC/DC converter to the SC, while a DC/AC converter is connected to the AC motor. The required power of this HEV is split by the proposed adaptive fuzzy energy management controller based on real time driving pattern recognition. The target vehicle is a VW Jetta modified hybrid vehicle in [36] whose main parameters are listed in TABLE I.

TABLE I
MAIN COMPONENTS AND PARAMETERS OF THE HEV

| Components | Parameters |
|------------------|--|
| Fuel cell | Rated power: 40 kW |
| Supercapacitor | Storage capacity: 160 Wh Power: 38 kW for a duration of roughly 15 s Single cell: rated capacitance 1700F rated voltage 2.5V Number of cells: 84 pairs in series Maximal voltage: 210V |
| DC/DC converters | Unidirectional DC/DC converter: 40kW,150A Bidirectional DC/DC converter: 40 kW, 150 A |
| Vehicle | Total vehicle mass: 2265 kg Frontal area *drag coefficient: 0.6 m ² Coefficient of rolling resistance: 0.1 |

B. Fuel cell

Proton exchange membrane fuel cells (PEMFC) can be operated at ambient temperatures with a short warm-up process, which makes them capable of following the dynamic load changes in the automotive applications. The output voltage of the fuel cell V_{act} is given as follows [37].

$$V_{out} = N_0 E_{cell} - V_{act} - V_{ohm} \quad (1)$$

$$V_{act} = B \ln(CI), V_{ohm} = IR_{ohm} \quad (2)$$

where E_{cell} , V_{act} , V_{ohm} are the Nernst cell voltage, activation voltage and the overall internal ohmic voltage, respectively. N_0 is the number of the fuel cells in series, B and C are constants used to calculate V_{act} , R_{ohm} is the internal resistance, and I is the output current of the FC. E_{cell} in (1) can be calculated as follows.

$$E_{cell} = E_{0cell}^0 - k_E (T - 298) + \frac{RT}{2F} \ln(p_{H_2} \sqrt{p_{O_2}}) - E_{dcell} \quad (3)$$

where p_{H_2} and p_{O_2} are the hydrogen and oxygen partial pressure [atm], which can be set as constants for simplicity. E_{0cell}^0 is the standard reference potential per cell. T is the temperature of the FC stack [K] and R is the gas constant. E_{dcell} in (3) is described by a first order transfer function as follows.

$$E_{dcell}(s) = \frac{\lambda_e \tau_e s}{\tau_e s + 1} I(s) \quad (4)$$

where λ_e and τ_e are a constant gain and the overall flow delay, respectively. The total hydrogen consumption in the reaction of the fuel cell can be derived as follows [37].

$$\dot{m}_{H_2} = \frac{M_{H_2} N_{cell} A_{FC}}{2F} I \quad (5)$$

where M_{H_2} is the molecular weight of the hydrogen, A_{FC} is the active area of each cell and F is the Faraday's constant. The parameters of a 40kW fuel cell are listed in TABLE II.

TABLE II
FUEL CELL SYSTEM PARAMETERS

| Name | Value | Unit |
|---|-----------------|-----------------|
| Number of cells N_0 | 750(375 series) | / |
| Activation voltage constant B | 0.0478 | / |
| Activation voltage constant C | 0.0136 | / |
| Standard reference potential per cell E_{0cell}^0 | 0.9 | v |
| Nominal operating temperature T | 368 | K |
| hydrogen partial pressure p_{H_2} | 2.0 | atm |
| oxygen partial pressure p_{O_2} | 2.2 | atm |
| Constant factor in E_{dcell} , λ_e | 0.00333 | / |
| Gas constant R | 8314.47 | / |
| Internal resistance R_{ohm} | 0.004 | Ω |
| Active area of each cell A_{FC} | 204 | cm ² |
| Faraday's constant F | 9.65e+4 | C/mol |

C. Power loaded supercapacitor

The RC model of the supercapacitor (SC) is relatively simple and can be obtained from the manufacturer datasheet. In addition, the current and voltage of the supercapacitor will change dynamically under different driving conditions, thus its resistor load is time-varying. To avoid estimating the dynamic resistor load, a supercapacitor connected to a power element P is shown in Fig.2 [38].

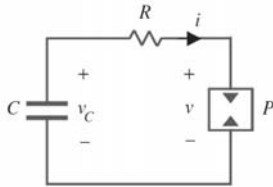


Fig. 2. RC model of Supercapacitor with power load

The terminal voltage v , the terminal current i and SC internal voltage v_c shown in Fig.2 satisfy the following formula.

$$i = -C \frac{dv_c}{dt} = \frac{v_c - v}{R} = \frac{P}{v} \quad (6)$$

Since the terminal voltage v is measurable, (6) can be further rewritten as

$$\frac{dv}{dt} + RP \frac{dv^{-1}}{dt} + \frac{P}{C} v^{-1} = 0 \quad (7)$$

If the load resistor is matched with the internal resistor R , the output power of SC can be maximized.

$$P_{max} = \frac{v^2}{R} = \frac{v_c^2}{R} \quad (8)$$

The state of charge (SOC) of the supercapacitor can also be derived as

$$SOC = \frac{v_c}{v_{max}} = \frac{v - iR}{v_{max}} \quad (9)$$

where $v_{min} \leq v \leq v_{max}$, v_{min} and v_{max} are the allowed minimal and maximal voltages of the SC, respectively.

III. GA BASED ADAPTIVE FUZZY ENERGY MANAGEMENT SYSTEM

A. Driving pattern recognition

For a determinate driving cycle, the number of the characteristic parameters can be as high as 62 [39]. However, the high dimension of the features is not helpful for real time driving pattern recognition. In [21], the features were decreased to 15. In [16], only two features, i.e., the maximal and average speeds, were used to classify driving patterns, however, the classification results were not consistent with the real driving conditions. Because the vehicle speed can be measured easily by the sensor, and the fuel consumption is mainly affected by the factors such as speed, speed variation, acceleration, stop, etc., 10 features among 15 characteristics in [21], its idle time and the number of stop/start, are listed in Table III. They are average speed (V_{avg}), maximal speed (V_{max}), standard deviation of speed (V_{std}), stop time (T_{idle}), number of stop/start (N_{stop}), maximal acceleration (A_{max}), maximal deceleration (D_{max}), maximal acceleration (A_{max}), maximal deceleration (D_{max}), maximal deceleration (D_{max}), extreme acceleration (A_{ext}), percentage of low speed time ($P_{low\ speed}$), percentage of high speed time ($P_{high\ speed}$), percentage of middle speed time ($P_{mid\ speed}$), respectively.

TABLE III.
STATISTICAL FEATURES OF 4 TYPICAL DRIVING PATTERNS

| Features | MBDC | UDDS | WVUSUB | HWFET |
|-------------------------------|---------|---------|---------|---------|
| V_{avg} (Km/h) | 39.4396 | 50.0956 | 53.9349 | 99.7451 |
| V_{max} (Km/h) | 10.9321 | 27.4094 | 26.2083 | 87.7848 |
| T_{idle} (s) | 53.7805 | 26.7627 | 36.5496 | 0.0652 |
| N_{stop} | 2.7317 | 2.1695 | 0.8092 | 0.0217 |
| A_{max} (m/s ²) | 5.9505 | 5.4798 | 3.2369 | 2.1026 |
| D_{max} (m/s ²) | -7.1202 | -5.2016 | -5.4768 | -3.2886 |
| A_{avg} (m/s ²) | 0.9933 | 1.1677 | 0.6821 | 0.4337 |
| D_{avg} (m/s ²) | -0.6999 | -0.9002 | -0.6253 | -0.4071 |
| A_{ext} (m/s ²) | 0.1601 | 0.1644 | 0.0547 | 0.0171 |
| $P_{low\ speed}$ (%) | 0.2372 | 0.1890 | 0.1133 | 0.0091 |
| $P_{mid\ speed}$ (%) | 0 | 0 | 0 | 0.5181 |
| $P_{high\ speed}$ (%) | 0 | 0 | 0 | 0.2184 |

To obtain the statistics features in Table III, the sampling window size T_{w1} and the updating window size T_{w2} should be set carefully in advance, which will lead to different feature value and may cause different classification results. In order to escape frequently mode switches, the sliding time window and updating time window for feature extraction are set as 150 and 50 seconds, respectively. Assuming that the current driving pattern keeps invariable before the next driving pattern recognition implementation, the parameters are determined by trials and errors from a number of simulation tests. It should be noted that the sliding time window for pattern recognition lasts for 150s and the driving pattern recognition is updated once every 50s. Thus, the sliding time window is moved with the updating window, e.g., the first sliding time window is [0, 150], the second is [50, 200], the third is [100, 250], etc. Congested urban roads, flowing urban roads, subway and highway are four typical driving patterns [31], which are divided by the Environmental Protection Agency (EPA) and represented as 1, 2, 3, 4, respectively. Manhattan bus drive cycle (MBDC), EPA urban dynamometer driving schedule (UDDS), West Virginia suburban driving schedule (WVUSUB) and US EPA highway fuel economy certification test (HWFET) are four typical corresponding driving conditions, which are labeled from 1 to 4 and used to be classified according to the extracted features. The features are then calculated and shown in Table III. Six features with quite different values among 4 driving patterns are selected, that is, V_{max} , V_{avg} , T_{idle} , A_{max} , D_{max} , $P_{low\text{speed}}$.

The neural network classifier is employed to recognize the driving patterns, as displayed in Fig. 3.

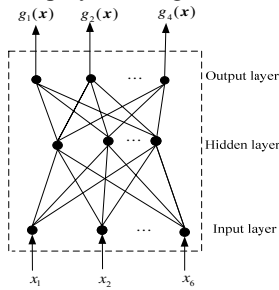


Fig. 3 A generic structure of an MLP NN classifier

The input layer has 6 nodes of the feature vector, $\mathbf{x} = [x_1, \dots, x_6]$, the hidden layer has n_H nodes and the output layer has 4 nodes with the discriminant function $g_1(\mathbf{x}), \dots, g_4(\mathbf{x})$. The activation function at the hidden layer is selected as the sigmoid function, $\phi(\xi) = \frac{1}{1 + \exp(-\xi)}$. The

multi-layered perceptron neural network with a single hidden layer and thresholds can approximate any function with a specified precision and the error back-propagation training algorithm is still adopted to this day [40].

The output of the i^{th} hidden node h_i from the input layer is processed as follows

$$h_i = \phi(\xi_i); \xi_i = \sum_{j=1}^6 w_{ij} x_j + w_{i0} \quad i=1, \dots, n_H \quad \mathbf{h} = [h_1, \dots, h_{n_H}] \quad (10)$$

where w_{ij} is the weight between the j^{th} input node and the i^{th} hidden node, w_{i0} is the threshold of the i^{th} hidden node. The output of the k^{th} output node can then be derived as

$$z_k = \sum_{j=1}^{n_H} w_{kj} h_j + w_{k0} \quad k=1, \dots, 4 \quad \mathbf{z} = [z_1, \dots, z_4] \quad (11)$$

where w_{kj} is the weight between the j^{th} hidden node and the k^{th} output node, w_{k0} is the threshold of the k^{th} output node. The classification error for the input feature vector is defined as the sum of the squared error between the labeled training set and the NN classifier output.

$$E = \sum_{k=1}^4 (z_k - c_k)^2 \quad \mathbf{c} = [c_1, \dots, c_4] \quad (12)$$

where c_k is a 4-component binary vector for the label (l_i), e.g., the 4-type classifier labels 1, 2, 3, 4, the binary vector of 1 is (0001), 2 is (0010), 3 is (0100) and 4 is (1000).

A gradient descent back-propagation algorithm is utilized to minimize the learning error E between the classifier output and the actual binary vector.

$$\begin{aligned} \Delta \mathbf{c} &= (\mathbf{z} - \mathbf{c}) * \mathbf{c} * (1 - \mathbf{c}) \\ \Delta \mathbf{h} &= \Delta \mathbf{c}' * \mathbf{W}_2 * \mathbf{h}' * (1 - \mathbf{h}') \end{aligned} \quad (13)$$

The weights from the output layer to the hidden layer, and the hidden layer to the input layer, are modified according to the learning error. Moreover, to improve the learning speed, a momentum term is added to the weight updating equation.

$$\begin{aligned} w_{ij}(t) &= w_{ij}(t-1) - \eta \Delta c_j \Delta h_i + \eta [w_{ij}(t-1) - w_{ij}(t-2)] \\ i &= 1, \dots, 4; j = 1, \dots, n_H \\ w_{jk}(t) &= w_{jk}(t-1) - \eta \Delta c_k \Delta h_j + \eta [w_{jk}(t-1) - w_{jk}(t-2)] \\ j &= 1, \dots, n_H; k = 1, \dots, 4 \end{aligned} \quad (14)$$

The update of the thresholds of the hidden and the output layers can also be obtained similarly.

$$\begin{aligned} w_{i0} &= w_{i0} - \eta \Delta h_i + \eta [w_{i0}(t-1) - w_{i0}(t-2)] \\ i &= 1, \dots, n_H \\ w_{k0} &= w_{k0} - \eta \Delta c_k + \eta [w_{k0}(t-1) - w_{k0}(t-2)] \\ k &= 1, \dots, 4 \end{aligned} \quad (15)$$

where η is the learning rate between (0,1).

Once the learning is iterated for K times for N training dataset: $\mathbf{X} = [\mathbf{x}_1, \dots, \mathbf{x}_N]$, $\mathbf{Y} = [l_1, \dots, l_N]$, the learning of the classifier is finished. If a new feature vector input appears, the NN classifier is to choose the maximal value among 4 output nodes.

$$l_o = \max(z_1, \dots, z_4) \quad (16)$$

B. Adaptive fuzzy energy management

The energy management controller in the HEV is to split the instantaneous power between the fuel cell and the supercapacitor, where its output gain can be changed adaptively based on real time driving patterns. The relationship between the energy management controller and driving pattern recognition is shown in Fig. 4, where the output of the fuzzy energy management controller is adjusted adaptively in terms of the recognized driving pattern using a neural network classifier. The classifier and the energy management controller are run independently, and the result of driving pattern recognition will influence the controller output.

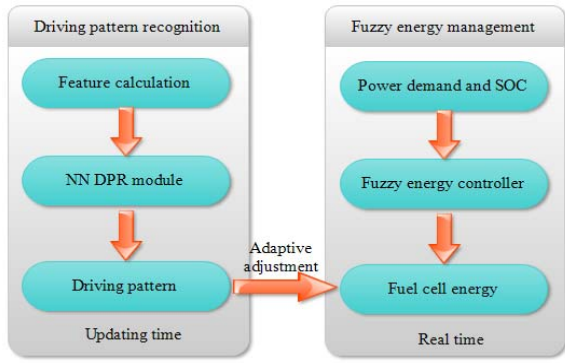


Fig.4 The framework of driving pattern recognition based fuzzy EMS.

Concretely, the structure of the basic fuzzy energy management controller is kept unchanged and only the output gain is adjusted corresponding to different driving patterns as shown in Fig. 5. To guarantee the safety of the supercapacitor, the energy management controller is executed when the demand power is positive and the SOC is larger than 0.7. If the SOC of supercapacitor is less than 0.5, the fuel cell provides all the required power at its subpower range.

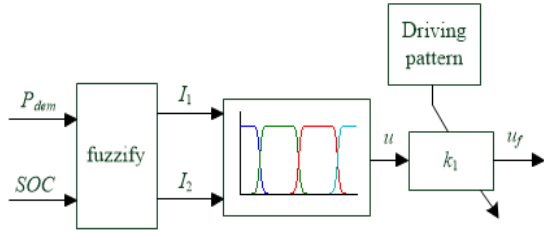


Fig. 5. Adaptive fuzzy energy management controller

The inputs of the fuzzy logic energy controller are the positive demand power P_{dem} required by the vehicle and the SOC of the supercapacitor, and the controller output is to assign the ratio of P_{dem} to the fuel cell.

After fuzzification, P_{dem} and SOC are changed into the fuzzy domain $[0, 1]$, $[0, 1]$, respectively.

$$\begin{cases} I_1 = \frac{P_{dem}}{P_{max}} \\ I_2 = \frac{SOC - SOC_{min}}{SOC_{max} - SOC_{min}} \end{cases} \quad (17)$$

where P_{max} is the maximal demand power, SOC_{max} , SOC_{min} are the maximal and minimal safe SOC.

In terms of expert knowledge about the energy management control system, the fuel cell's power source delivers as much as possible the requested power when the demand power is high and the SOC of the supercapacitor is low. When the demand power is low and the SOC of the supercapacitor is high, the fuel cell stack delivers low power. One example of the expert rule is: if the demand power I_1 is High and SOC I_2 is low (L), then u_f is high (H).

TABLE IV:
FUZZY LOGIC RULES

| $u_f \backslash P_{dem}$ | VL | L | M | H |
|--------------------------|----|----|----|----|
| SOC | | | | |
| L | L | M | MH | H |
| M | ML | L | M | MH |
| H | VL | ML | L | M |

The whole rule base obtained by expert experience is listed in Table IV, where the demand power is divided into 4 fuzzy linguistic domains: 'very low' (VL), 'low' (L), 'Medium' (M) and 'high' (H), while the SOC is divided into 3: 'low' (L), 'Medium' (M) and 'high' (H). The output power of the fuel cell can be 'very low' (VL), 'medium low' (ML), 'low' (L), 'medium' (M), or 'medium high' (MH) and 'high' (H). Each linguistic value is assigned by a membership function. Here, a Gaussian membership function (MF) has been selected over the universe discourse, which is $Gaussian(x; \sigma, c) = \exp(-\|x - c\|^2 / 2\sigma^2)$, where c represents MF's center and σ determines MF's width. A group of typical expert fuzzy membership functions for SOC , P_{req} and u_f are shown in Fig.6, where the membership functions in different fuzzy linguistic domain are distinct from other colors.

Using centroid defuzzification, the fuzzy controller output can be formulated as follows [41]

$$u_f(k) = \frac{\sum_{j=1}^{r_1} \sum_{i=1}^{r_2} \mu_{I_1}^j(k) \mu_{I_2}^i(k) \Delta \mu_u^{ij}(k)}{\sum_{j=1}^{r_1} \sum_{i=1}^{r_2} \mu_{I_1}^j(k) \mu_{I_2}^i(k)} \quad (18)$$

where r_1 and r_2 are the numbers of the fuzzy linguistic division, $\mu_x(k)$ is the degree of the membership function of SOC and P_{dem} , respectively, $\Delta \mu_u^{ij}(k)$ is obtained using Mamdani product and the max fuzzy inference scheme.

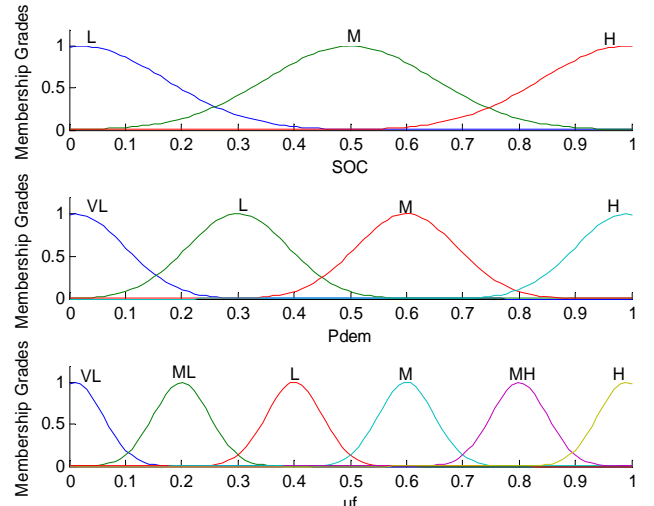


Fig. 6 Membership functions for inputs and outputs of FLC

The coefficient k_1 in Fig.5 is then modified according to four types of driving patterns, denoted as a vector \mathbf{k}

$$\mathbf{k} = [k_1, k_2, k_3, k_4] \quad (19)$$

The coefficient in the above vector is selected adaptively for real time driving pattern recognition, which will be added to the fuzzy controller output u_f , and the fuel cell power is derived as

follows

$$P_f = (u_f + k(i))P_{dem} \quad i=1,4 \quad (20)$$

where the split coefficient is less than 1. We observe that the coefficients in k will affect the ultimate splitting result directly and must be carefully defined through experiments.

C. The objectives of optimization

For an adaptive fuzzy EMS, fuel consumption must be minimized so that the lifecycle of fuel cells can be prolonged. Violent load variation usually affects the lifetime of fuel cells tremendously, leading to current and voltage fluctuations of fuel cells. Hence, the objectives of the adaptive fuzzy EMS are to minimize both the fuel consumption and current fluctuation simultaneously. In addition, constraints have to be satisfied to guarantee the safety of the energy system. For example, to avoid reactant starvation, the maximal current in a fuel cell is limited to 150 A. Because of the chemical response lag of the reactant supply system, the power change rate of the fuel cell is restricted to 5 kW/s. Once the stack voltage falls below 60 V, a fuel cell will be shut down. As for supercapacitors, their transient power is limited to 30 kW and the current is less than 150A considering the power of a bidirectional DC/DC converter. To avoid overcharging, once its maximal voltage is reached, the charging is turned off. The SOC of the supercapacitor is kept in the range of [0.5 1] in order to absorb the regenerative braking power and to provide sufficient transient power. Mathematically, the optimization problem for balancing the energy consumption and system safety can be **formulated** using a weighted sum of objectives method.

$$\begin{aligned} \text{Min } J &= \omega \sum_{j=1}^K \Delta I_j^2 + \sum_{j=1}^K m_{H_2} \\ \text{s.t. } P_{FC} + P_{SC} &= P_{dem} \\ 0 < P_{FC} &\leq 40 \\ 0 < i_{FC} &\leq 150 \\ -5 \leq \Delta P_{FC} &\leq 5 \\ -30 \leq P_{SC} &\leq 30 \\ -150 \leq i_{SC} &\leq 150 \\ 0.5 \leq SOC &< 1 \\ v_{FC} \geq 60 \end{aligned} \quad (21)$$

where ΔI_j is the current variance of the fuel cell, K is the number of the samples in the whole driving trip, P_{FC} is the output power of the fuel cell, P_{SC} is the power provided by the supercapacitor, ΔP_{FC} is the power variation of the fuel cell, and ω is the weight coefficient of the two objectives. The inequality and equality constraints are handled as penalty factors added to J .

D. GA based adaptive fuzzy EMS

The relationship between the objective and the parameters of the adaptive energy management controller cannot be fully described by a mathematical formulation, which is difficult to be solved by traditional optimization methods. A genetic algorithm (GA) is hence adopted to optimize the parameters in the fuzzy energy management controller.

Genetic encoding

The adaptive gains and the parameters of the membership functions are optimized by GA. As described in Section 3.2, totally seven membership functions from the two inputs and six membership functions from the output result in 26 parameters of the fuzzy controller to be optimized. For simplification, the width is set to be the type of the variables. Hence, there are sixteen parameters out of the fuzzy controller and four adaptive coefficients to be optimized. The i^{th} chromosome (C_i) using the decimal encoding is then given as follows

$$\begin{aligned} C_i &= [c_{i1}, \dots, c_{ji}, \dots, c_{20i}] \\ &= [c_{i1}, \dots, c_{13i}, \sigma_{1i}, \sigma_{2i}, \sigma_{3i}, k_{1i}, k_{2i}, k_{3i}, k_{4i}] \end{aligned} \quad (22)$$

$$i = 1, 2, \dots, N$$

where N is the population size. The elements in (22) are initialized randomly between $[min, max]$.

$$c_{j,i} = \min + \delta \cdot (\max - \min) \quad 1 \leq j \leq 20 \quad (23)$$

where δ is generated between (0,1) randomly.

Genetic Operators

Three operators, i.e., selection, crossover and mutation, will be adopted to help finding an optimal solution.

(1) Selection

Roulette wheel selection is widely used in GA and the probability distribution is computed in terms of the value of the objective function.

$$p = [p_1, \dots, p_N] = \left[\frac{f_1}{\sum_{i=1}^N f_i}, \frac{f_1 + f_2}{\sum_{i=1}^N f_i}, \dots, \frac{\sum_{i=1}^{N-1} f_i}{\sum_{i=1}^N f_i}, 1 \right] \quad (24)$$

where $f_i = 1/J_i$, and J_i is the value of the objective function with necessary constraints for the i^{th} individual. A random number γ between (0, 1) is generated, then individuals satisfying $\gamma < p_i$ can be found, however, only one individual at the first index is selected as the parent. Totally $N-1$ Roulette wheel selections are executed and the elitism is maintained in the parents.

(2) Crossover and mutation operators

Crossover operation is executed with probability p_c between individuals C_i and C_{i+1} . The offspring C'_i , C'_{i+1} are then generated as

$$\begin{aligned} C'_i &= \alpha C_i + (1-\alpha)C_{i+1} \\ C'_{i+1} &= \alpha C_{i+1} + (1-\alpha)C_i \end{aligned} \quad (25)$$

where α is selected randomly in the range of (0,1).

For a better exploration, a mutation operator is carried out among N offsprings with probability p_m . Once the element c_{ji} in C'_i is mutated, new element c'_{ji} is then produced according to (23).

E. Processes of the proposed algorithm

Neural network (NN) learning and GA optimization processes are undertaken offline. The learning process of the neural network is summarized as follows:

Step 1: Set the number of the hidden nodes, the sampling window size T_{w1} and the updating window size T_{w2} , the learning rate η , the error goal $\epsilon > 0$, and the number of the training epochs N_n . Initialize all the weights

including biases of the neural network randomly in the range of $(0, 1)$.

Step 2: Calculate the output of the NN classifier with the current weights by forward propagation and obtain error E in terms of (12).

Step 3: Compute the error term of each node of the output layer and the hidden layer according to (13).

Step 4: For each hidden and output node, update the weights using the learning rate η in terms of (14).

Step 5: Repeat steps 2 to 4 till E satisfies the pre-defined threshold or the training epochs are reached.

Thus, the neural network classifier is learned, where the weights and the hidden layer are fixed, and only the forward propagation is utilized for real time driving pattern recognition in the GA optimization process, which is shown as follows.

Step 1: Initialize the maximal generation G , population size N , crossover and mutation operator probabilities p_c , p_m and its weight coefficient ω . Initialize the chromosomes in the search space randomly.

Step 2: For each chromosome, generate features and identify the current driving pattern using a neural network classifier; apply the adaptive fuzzy energy management controller and obtain the performance J .

Step 3: Produce the offspring using a standard tournament selection and elitism strategy. Execute crossover and mutation operation with probability p_c and p_m , respectively.

Step 4: Repeat steps 2 to 3 till the maximal evolution generation G is obtained.

After the offline optimization of GA, the adaptive fuzzy energy management is achieved, which can be used online for testing.

IV. SIMULATION RESULTS

A. Real world driving pattern recognition

The typical driving patterns presented in section 3.1 consist of: MBDC, UDDS, WVUSUB and HWFET, which are used to train the neural network classifier and the adaptive fuzzy energy management controller by GA, whose speed distribution is shown in Fig.7. The parameters of the neural network classifier are set as follows: the learning rate is 0.2, the error goal ϵ is 0.001, and the number of the training epochs N_n is 1000. There are totally 4612 speed samples shown in Fig.7, where the sampling period is 1 sec.

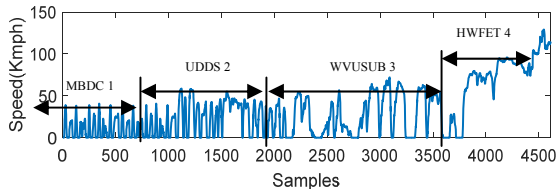


Fig.7. Four typical vehicle driving speed distribution for training neural network.

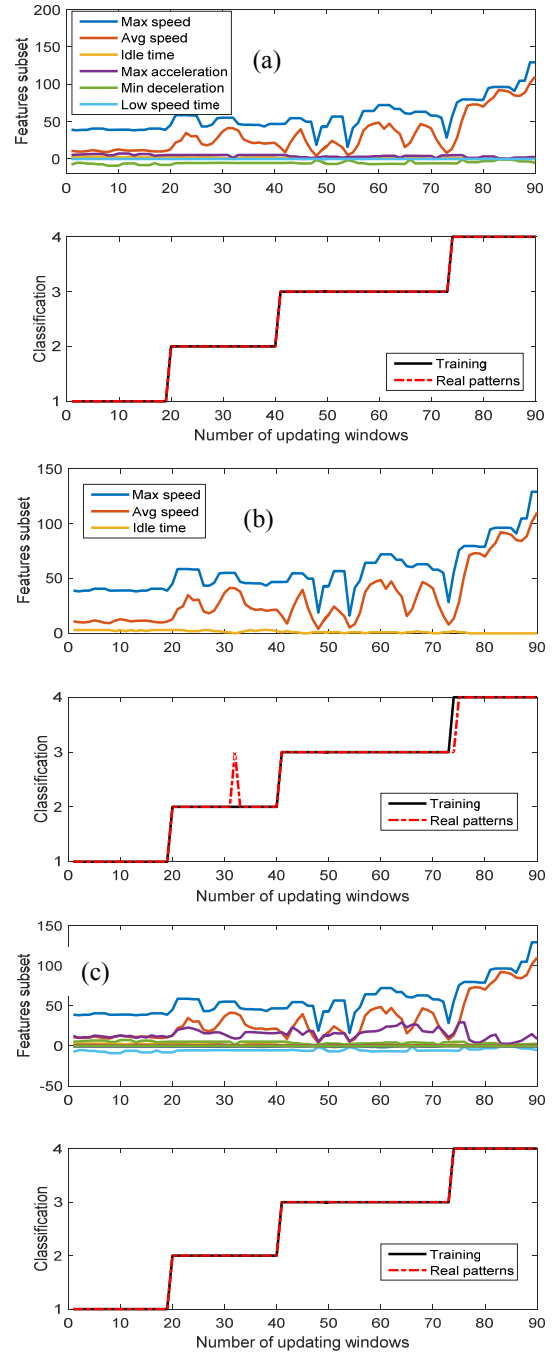


Fig.8. The feature extraction and training results of neural network (a) 6 features (b) 3 features (c) 12 features.

To show the effect of different numbers of the extracted features, 12 features and 3 features are used as an example to compare the system performance. Here, about 90 sliding time windows are extracted and the features and its classified results are shown in Fig.8. We notice that both 12 features and 6 features can lead to satisfactory training results, but there exist some errors in the case of 3 features. After the offline training, the neural network classifier is then used to identify the driving patterns online. NewYork Bus cycles, UDDS, Urban driving cycle (UDC), Extra urban driving cycle (EUDC), and US06 high way form the test inputs, as illustrated in Fig.9. They

represent the congested and flowing urban driving, suburb driving and highway driving patterns individually and are labeled as 1, 2, 3 and 4, respectively.

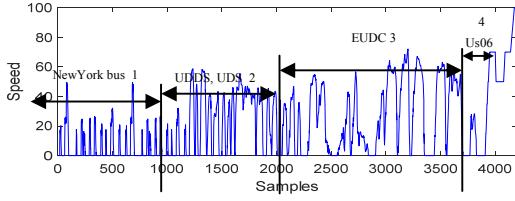


Fig.9. A hybrid of 4 types driving patterns for testing the classifiers.

TABLE V

ACCURACY COMPARISON WITH DIFFERENT FEATURES

| Accuracy | 3 features | 6 features | 12 features |
|----------|------------|------------|-------------|
| Train(%) | 97.78 | 100 | 100 |
| Test(%) | 83.55 | 95.82 | 86.27 |

TABLE VI

FALSE ALARM RATE COMPARISON WITH DIFFERENT FEATURES

| False alarm rate | 3 features | 6 features | 12 features |
|------------------|------------|------------|-------------|
| Train(%) | 2.82 | 0 | 0 |
| Test(%) | 22.51 | 6.22 | 26.13 |

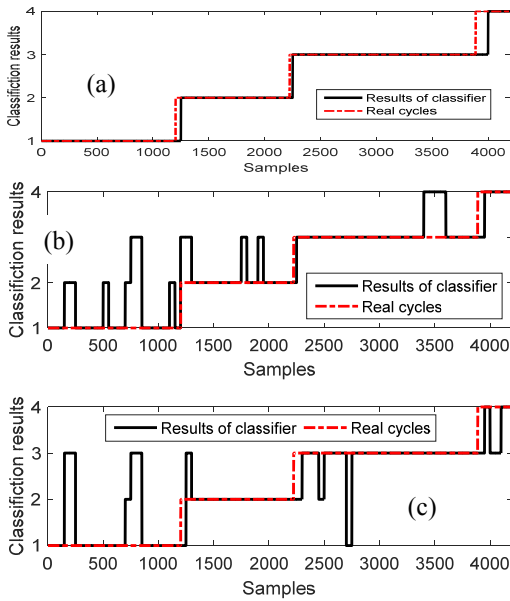


Fig.10. Real time neural network classifying results (a) 6 features (b) 3 features (c) 12 features.

B. GA optimized adaptive fuzzy EMS

The parameters of GA are set as follows: $N=60$, $G=100$, $p_c=0.9$ and $p_m=0.1$, the weight ω is set as 0.3 by trial and error, and the SOC of the supercapacitor is initialized as 0.8. The value of min and max are set as 0.01 and 1, respectively. GA is run at a notebook with Intel Core i5-3470 @ 3.2GHz and 4G RAM for 10 times. The adaptive fuzzy EMS with the minimal value of the objective function is selected to split the power required by the driving cycles.

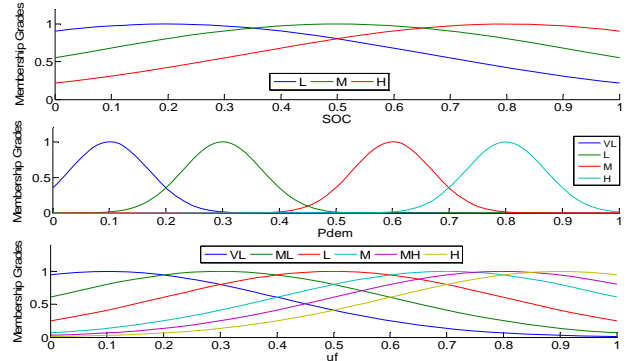


Fig.11 The optimized fuzzy membership functions

After optimization, the output coefficient k is obtained as [0.0926 0.4407 0.4083 0.6041]. Their membership functions are plotted in Fig.11, which is obtained automatically by GA and different to those in Fig.6. The fuzzy inference and defuzzification discussed in section 3.2 are utilized and the control surfaces covering all the conditions of P_{dem} and SOC are shown in Fig.12, which is consistent with the fuzzy rules in Table IV and the output surface is varying with different driving patterns. However, the output surfaces for the flowing urban roads and subways are very close.

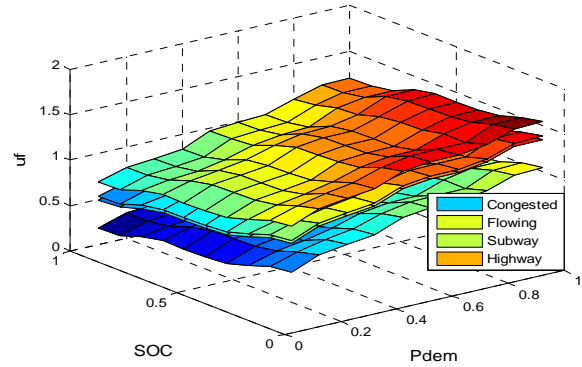


Fig.12 The control surface of defuzzification output for 4 driving patterns

C. Performances comparison

To show the efficiency of the proposed method, the fuzzy EMS without adaptation but optimized by the same objective function and the adaptive fuzzy EMS only aiming at fuel minimization are chosen to be compared. After optimization, k_1 in the fuzzy EMS without adaptation is 0.5528. k in the H_2 consumption minimization based adaptive fuzzy EMS is optimized as [0.3765 0.3683 0.5017 0.5649], and the membership functions in the two methods are the same as the proposed fuzzy EMS. Note that the adaptive coefficients for congested and flowing urban roads are almost identical.

The utilization percentage of the fuel cells, root mean square error (RMSE) of currents and voltage perturbation in the fuel cells and the RMSE of the demanding power are important performance indices and are listed in Table V for the training and testing data. The utilization percentage of the fuel cell during the whole cycle is defined as follows [42]

$$Utilization(\%) = \frac{\int_{cycle} P_{FC}(t) dt}{\int_{cycle} P_{FC}(t) dt + \int_{cycle} P_{SC}(t) dt} \times 100 \quad (26)$$

TABLE V:
THE COMPARISON OF THE SIMULATION RESULTS FOR 3 METHODS

| Traffic condition | Proposed fuzzy EMS | | | | fuzzy EMS without adaptation | | | | Adaptive fuzzy EMS min H ₂ | | | |
|-------------------|--------------------|-------------|----------------|-------------------------|------------------------------|-------------|----------------|-------------------------|---------------------------------------|-------------|----------------|-------------------------|
| | FC | RMSE(I,V) | H ₂ | RMSE(P _{dem}) | FC | RMSE(I,V) | H ₂ | RMSE(P _{dem}) | FC | RMSE(I,V) | H ₂ | RMSE(P _{dem}) |
| Training | 87% | (11.8,11.4) | 0.587 | 7.98e-14 | 88% | (12.2,11.9) | 0.597 | 8.14e-14 | 87% | (12.2,11.1) | 0.584 | 3.8e-14 |
| Testing | 89% | (12.2,13.1) | 0.41 | 6.08e-14 | 90% | (13.9,14.6) | 0.45 | 7.73e-14 | 88% | (13.4,14.1) | 0.44 | 4.61e-14 |

It can be seen that the demanding power can be satisfied for both the training and testing data by all the methods, where the RMSE is of the order of 10^{-14} . For the training data, the adaptive fuzzy EMS minimizing the H₂ consumption has obtained the least fuel consumption, while the proposed method has led to the smallest fluctuation of currents and voltages for the fuel cells and the fuzzy EMS without adaptation results in the worst performance. The system performance difference is not significant because all the methods adopt the same fuzzy rules and all the parameters of the fuzzy EMS are optimal by GA. As for the testing data, 8.89% of the fuel consumption is saved by the proposed method, compared with the fuzzy EMS without adaptation. The least RMSE of current and voltage variation are reached by the proposed fuzzy EMS, and up to 12.23% current variant has been decreased, compared with the fuzzy EMS without adaptation. With regard to the total fuel consumption, the adaptive fuzzy EMS minimizing H₂ requests the lowest. However, the improvement of the FC utilization percentage (88% to 89%) is minor. Similarly, the fuzzy EMS without adaptation has the largest current and voltage fluctuation.

The differences between the demand power of the HEV and the hybrid FC/SC power output for the training and testing data in the typical traffic conditions are shown in Fig. 13. It is noticed that the error distribution is consistent with the statistical root mean square errors and the fuzzy energy management controller can satisfy the required power at different driving patterns. The power split results of the supercapacitor by the three methods are depicted in Fig. 14. Here, the negative power means that the supercapacitor has absorbed the brake energy, which is utilized to drive the vehicle and **beneficial** for saving the H₂ consumption. However, most of the required power is provided by the fuel cells, as shown in Fig. 15, and is consistent with more than 85% of the utilization percentage of the fuel cell shown in Table V. The supercapacitor only acts as the auxiliary power to compensate for the instantaneous power and absorb the brake energy.

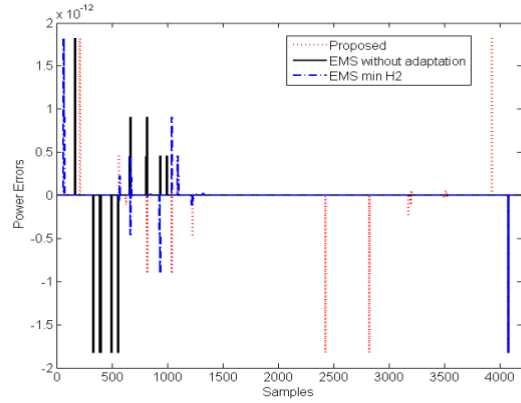


Fig. 13 The power error distribution for (a) training data and (b) testing data.

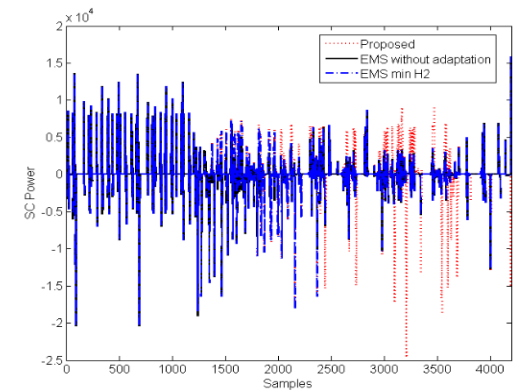
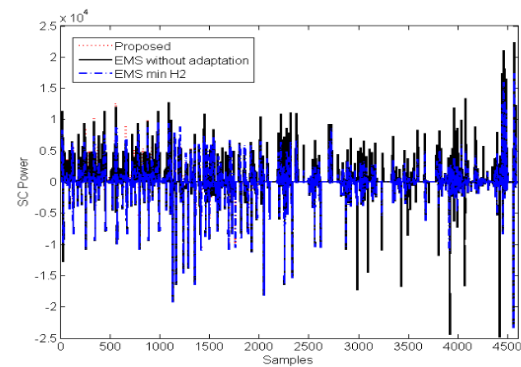
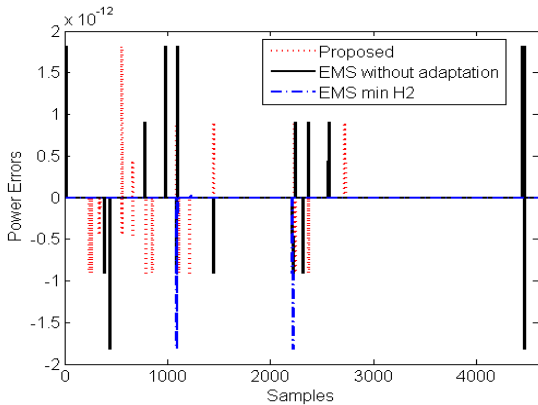


Fig. 14 The power provided by the supercapacitor for (a) training data and (b) testing data.



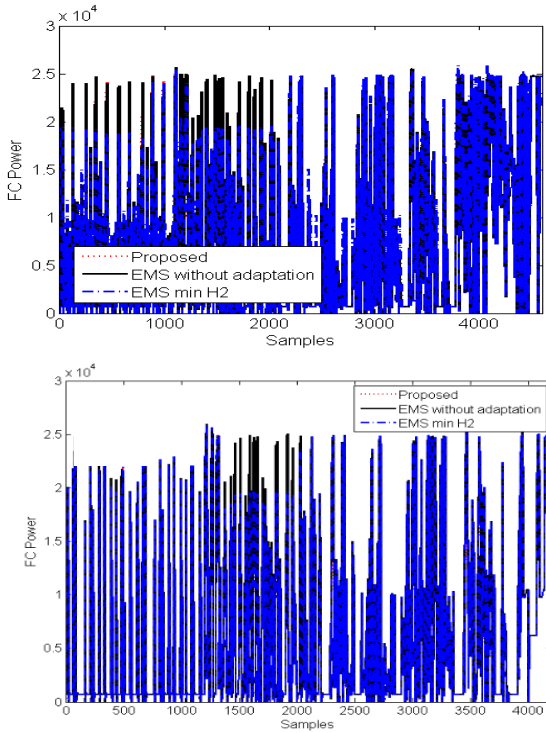


Fig.15 The power provided by the fuel cell for (a) training data and (b) testing data.

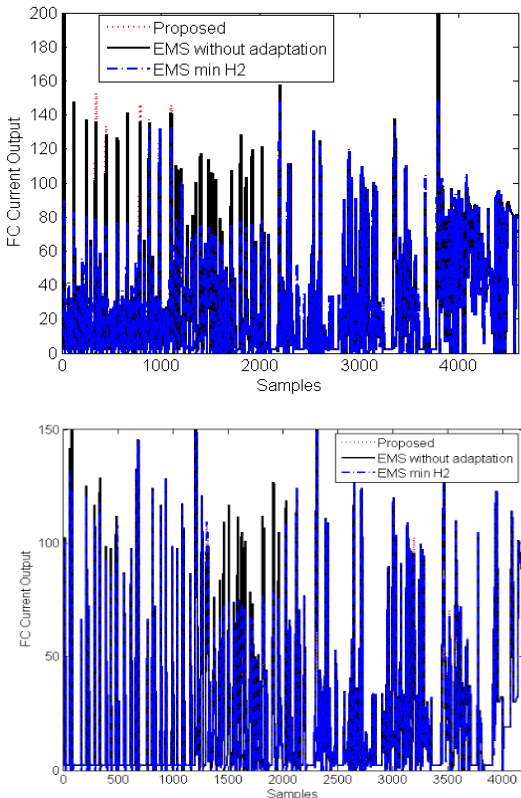


Fig.16 The current output of the fuel cell for (a) training data and (b) testing data.

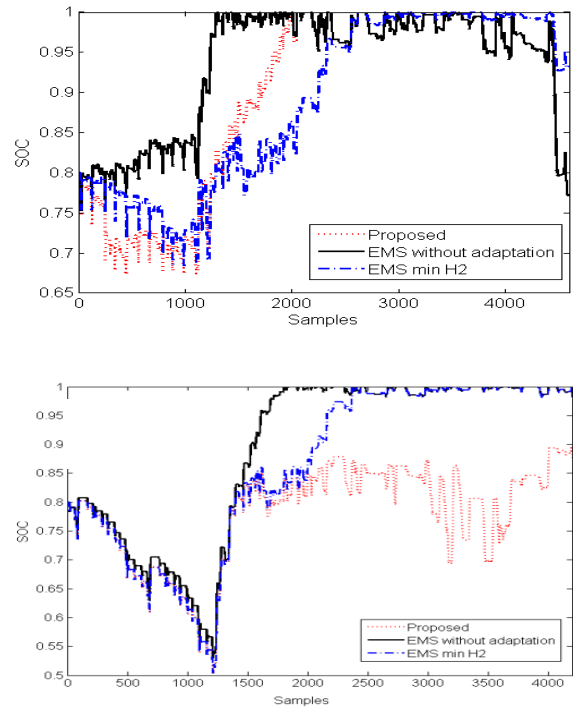


Fig.17 The state of the charge of the supercapacitor for (a) training data and (b) testing data.

The currents of the fuel cells obtained by the three fuzzy EMSs are compared and shown in Fig.16. It can be seen that though there are a few points of larger fluctuations in the training data, the fluctuation decreases in the testing case partly because of the compensation of the supercapacitor as shown in Fig.15(b). The current fluctuation using the fuzzy EMS without adaptation is much larger than that of the other two methods. The SOC of the supercapacitor is shown in Fig. 17, where it is among the safe range: [0.5,1], and the SOC of the proposed fuzzy EMS is much smaller than those of the other methods in the testing cases. This is consistent with the case of the smallest H₂ consumption because the supercapacitor provides more power to decrease the fuel consumption. In the case of training conditions, the fuzzy EMS minimizing H₂ consumption obtained the lowest SOC with the least H₂ consumption.

V. CONCLUSION

In the proposed adaptive fuzzy EMS, very little expert knowledge is required to define the fuzzy rules and a GA was proposed to automatically determine the adaptive coefficients of the EMS in different driving patterns and the parameters of fuzzy membership functions. No driving pattern is required in advance, which is obtained by a neural network classifier online in terms of real time applications. Up to 95% test accuracy has been obtained by the neural network classifier. The perturbation of the output current and voltage are minimized and this prolongs the lifetime of the fuel cell. Minimal fuel consumption was gained and the voltage and current fluctuations of the fuel cell were decreased remarkably in the simulation comparison with the expert fuzzy EMS and adaptive fuzzy EMS min H₂ on different driving patterns. The characteristics of the quick charge and discharge of the

supercapacitor are utilized adequately and the slow response and hydrogen starvation of the fuel cell can be compensated for by the SC bank during the transient variation of the required power. Although the neural network classifier can online recognize four driving patterns correctly, the adaptive coefficients, e.g., in the case of subways and flowing urban roads, are quite similar, which request less energy management. In the future, research studies on the relationship between classifiers and the energy management controller will be carried out to decrease the controller gain switch and make the energy management system applicable to more complicated conditions.

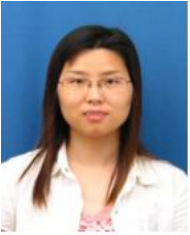
REFERENCES

- [1] X. Li, *Principles Fuel Cells*, Taylor & Francis, US, 2006.
- [2] J. R. Meacham, F. Jabbari, J. Brouwer, J. L. Mauzey, and G. S. Samuelson, "Analysis of stationary fuel cell dynamic ramping capabilities and ultra capacitor energy storage using high resolution demand data," *J. Power Sources*, vol. 156, no. 2, pp. 472-479, Jun. 2006.
- [3] A. Khaligh and Z. Li, "Battery, ultracapacitor, fuel cell, and hybrid energy storage systems for electric, hybrid electric, fuel cell, and plug-in hybrid electric vehicles: State of the art," *IEEE Trans. Veh. Technol.*, vol. 59, no. 6, pp. 2806-2814, Jul. 2010.
- [4] M. J. Kim and H. Peng, "Power management and design optimization of fuel cell/battery hybrid vehicles," *J. Power Sources*, vol. 165, no. 2, pp. 819-832, Mar. 2007.
- [5] C. Liu, Z. Yu, D. Neff, A. Zhamu, and B. Z. Jang, "Graphene-based supercapacitor with an ultrahigh energy density," *Nano letters*, vol. 10, no. 12, pp. 4863-4868, Nov. 2010.
- [6] Q. Li, W. Chen, Z. Liu, M. Li, and L. Ma, "Development of energy management system based on a power sharing strategy for a fuel cell-battery-supercapacitor hybrid tramway," *J. power sources*, vol. 279, no. 1, pp. 267-280, Apr. 2015.
- [7] W. W. Xiong, Y. hang, and C. L. Yin, "Configuration design, energy management and experimental validation of a novel series-parallel hybrid electric transit bus," *J. Zhejiang University Sci. A*, vol. 10, no. 9, pp. 1269-1276, Nov. 2009.
- [8] O. Madani, A. Bhattacharjee, and T. Das, "Decentralized Power Management in a Hybrid Fuel Cell Ultracapacitor System," *IEEE Trans. Control Syst. Techn.*, vol. 24, no. 3, pp. 765-778, May. 2016.
- [9] D. Fares, R. Chedid, F. Panik, S. Karaki, and R. Jabr, "Dynamic programming technique for optimizing fuel cell hybrid vehicles," *Int. J. Hydrogen Energ.*, vol. 40, no. 24, pp. 7777-7790, Jun. 2015.
- [10] A. Panday and H. O. Bansal, "Energy management strategy for hybrid electric vehicles using genetic algorithm," *J. Renew. Sustain. Energ.*, vol. 8, no. 1, pp. 741-746, Jan. 2016.
- [11] M. K. Dayeni and M. Soleymani, "Intelligent energy management of a fuel cell vehicle based on traffic condition recognition," *Clean Technol. Environ. Policy*, vol. 18, no. 6, pp. 1945-1960, Aug. 2016.
- [12] L. Wu, Y. Wang, X. Yuan, and Z. Chen, "Multiobjective optimization of hev fuel economy and emissions using the self-adaptive differential evolution algorithm," *IEEE Trans. Veh. Technol.*, vol. 60, no. 6, pp. 2458-2470, Jul. 2011.
- [13] D. F. Opila, X. Wang, R. Mcgee, and R. B. Gillespie, "An energy management controller to optimally trade off fuel economy and drivability for hybrid vehicles," *IEEE Trans. Control Syst. Techn.*, vol. 20, no. 6, pp. 1490-1505, Nov. 2012.
- [14] S. Zhang, X. Rui, and C. S. Feng, "Model predictive control for power management in a plug-in hybrid electric vehicle with a hybrid energy storage system," *Appl. Energ.*, vol. 185, no. 2, pp. 1654-1662, Jan. 2017.
- [15] J. Moreno, M. E. Ortuzar, and J. W. Dixon, "Energy-management system for a hybrid electric vehicle, using ultracapacitors and neural networks," *IEEE Trans. Ind. Electron.*, vol. 53, no. 2, pp. 614-623, Apr. 2006.
- [16] H. Hemi, J. Ghouili, and A. Cheriti, "A real time fuzzy logic power management strategy for a fuel cell vehicle," *Energ. Conv. Manage.*, vol. 80, no. 4, pp. 63-70, Apr. 2014.
- [17] M. C. Kisacikoglu, M. Uzunoglu, and M. SA. lam, "Load sharing using fuzzy logic control in a fuel cell/ultracapacitor hybrid vehicle," *Int. J. Hydrogen Energ.*, vol. 34, no. 3, pp. 1497-1507, Feb. 2009.
- [18] O. Erdinc, B. Vural, and M. Uzunoglu, "A wavelet-fuzzy logic based energy management strategy for a fuel cell/battery/ultra-capacitor hybrid vehicular power system," *J. Power Sources*, vol. 194, no. 1, pp. 369-380, Oct. 2009.
- [19] S. Berrazouane and K. Mohammadi, "Parameter optimization via cuckoo optimization algorithm of fuzzy controller for energy management of a hybrid power system," *Energ. Conv. Manage.*, vol. 78, no. 1, pp. 652-660, Feb. 2014.
- [20] T. Fletcher, R. Thring, and M. Watkinson, "An energy management strategy to concurrently optimise fuel consumption & PEM fuel cell lifetime in a hybrid vehicle," *Int. J. Hydrogen Energ.*, vol. 41, no. 46, pp. 21503-21515, Aug. 2016.
- [21] L. Feng, W. Liu, and B. Chen, "Driving pattern recognition for adaptive hybrid vehicle control," *SAE Int. J. Altern. Powertrains*, vol. 1, no. 1, pp. 169-179, Jan. 2012.
- [22] D. A. Johnson and M. M. Trivedi, "Driving style recognition using a smartphone as a sensor platform," *IEEE Intell. Trans. Syst. Mag.*, pp. 1609-1615, Oct. 2011.
- [23] L. Stenneth, O. Wolfson, P. S. Yu, and B. Xu, "Transportation mode detection using mobile phones and GIS information," *Proc. ACM SIGSPATIAL Int. Conf. Adv. Geogr. Inform. Syst.*, pp. 54-63, Nov. 2011.
- [24] Q. Gong, Y. Li, and Z. R. Peng, "Optimal power management of plug-in HEV with intelligent transportation system," *IEEE Int. Conf. Adv. Intell. Mechtron.*, pp. 1-6, Dec. 2007.
- [25] B. Y. Liaw, "Fuzzy logic based driving pattern recognition for driving cycle analysis," *J. Asia. Elec. Veh.*, vol. 2, no. 1, pp. 551-556, Jun. 2004.
- [26] J. Wang, Q. N. Wang, X. H. Zeng, and P. Y. Wang, "Driving cycle recognition neural network algorithm based on the sliding time window for hybrid electric vehicles," *Int. J. Auto. Tech.*, vol. 16, no. 4, pp. 685-695, Mar. 2015.
- [27] J. Wang, Y. Huang, H. Xie, and G. Tian, "Driving Pattern Recognition and Energy Management for Extended Range Electric Bus," *IEEE Veh. Power Propul. Conf.*, pp. 1938-8756, Feb. 2015.
- [28] X. Zhang, G. Wu, Z. Dong, and C. Crawford, "Embedded feature-selection support vector machine for driving pattern recognition," *J. Franklin Inst.*, vol. 352, no. 2, pp. 669-685, Feb. 2015.
- [29] M. Marx and D. Söffker, "A New Optimal Power and Energy Management Approach Applied to a Fuel Cell/Supercap Based Hybrid Powertrain System," *Joint Conf. Mov. ASME DSCC*, pp. 779-783, Oct. 2012.
- [30] E. Demeester, A. Hüntemann, D. Vanhooydonck, G. Vanacker, H. Van Brussel, and M. Nuttin, "User-adapted plan recognition and user-adapted shared control: a Bayesian approach to semi-autonomous wheelchair driving," *Auton. Robots*, vol. 24, no. 2, pp. 193-211, Feb. 2008.
- [31] S. Zhang and R. Xiong, "Adaptive energy management of a plug-in hybrid electric vehicle based on driving pattern recognition and dynamic programming," *Appl. Energ.*, vol. 155, pp. 68-78, Oct. 2015.
- [32] R. Zhang, J. Tao, "A nonlinear fuzzy neural network modeling approach using improved genetic algorithm," *IEEE Trans. Ind. Electron.*, vol. 65, no. 7, pp. 5882-5892, Jul. 2018.
- [33] L. I. Kuncheva, *Ensemble Methods. Combining Pattern Classifiers: Methods and Algorithms*, Second Edition. John Wiley & Sons, 2014.
- [34] R. Zhang, J. Tao, and F. Gao, "Temperature modeling in a coke furnace with an improved RNA-GA based RBF network," *Ind. Eng. Chem. Res.*, vol. 55, no. 8, pp. 3236-3245, Feb. 2014.
- [35] T. Markel, A. Brooker, T. Hendricks, V. Johnson, K. Kelly, and B. Kramer, "ADVISOR: a systems analysis tool for advanced vehicle modeling," *J. Power Sources*, vol. 110, no. 2, pp. 255-266, Aug. 2002.
- [36] S. Caux, W. Hankache, M. Fadel, and D. Hissel, "On-line fuzzy energy management for hybrid fuel cell systems," *Int. J. Hydrogen Energ.*, vol. 35, no. 5, pp. 2134-2143, Mar. 2010.
- [37] C. Qi and H. X. Li, "A time/space separation-based hammerstein modeling approach for nonlinear distributed parameter processes," *Comput. Chem. Eng.*, vol. 33, no. 7, pp. 1247-1260, Jul. 2009.
- [38] Z. L. Cheng, W. R. Chen, Q. Li, and Z. L. Jiang, "Modeling and Dynamic Simulation of an Efficient Energy Storage Component- Supercapacitor," *IEEE Asia-Pacific Power Eng. Eng. Conf.*, pp. 1-4, Apr. 2010.
- [39] E. Ericsson, "Independent driving pattern factors and their influence on fuel-use and exhaust emission factors," *Transp. Res. PT D Transp. Environ.*, vol. 6, no. 5, pp. 325-345, Sep. 2001.
- [40] B. D. Ripley, *Pattern recognition and neural networks*, Cambridge University Press, CO, 2015.
- [41] D. S. Ernest Czogała, *Fuzzy and Neuro-Fuzzy Intelligent Systems*. Physica-Verlag, GER, 2000.
- [42] V. Paladini, T. Donato, and A. D. Risi, "Super-capacitors fuel-cell hybrid electric vehicle optimization and control strategy development," *Energ. Conv. Manage.*, vol. 48, no. 11, pp. 3001-3008, Nov. 2007.



Ridong Zhang received the Ph.D. degree in control science and engineering from Zhejiang University, Hangzhou, China, in 2007. He is currently a Professor with the Institute of Information and Control, Hangzhou Dianzi University, Hangzhou. From 2012 to 2016, he was a visiting professor at the Chemical and Biomolecular Engineering Department, The Hong Kong University of Science and Technology, Hong Kong. His research interests include process modeling, process control and

nonlinear systems.



Jili Tao received the B.Sc. degree in communication engineering and the M.Sc. degree in traffic information engineering and control from Central South University, Changsha, China, in 2001 and 2004, respectively, and the Ph.D. degree in control science and control engineering from Zhejiang University, Hangzhou, China, in 2007. She is currently a Professor in the Institute of Ningbo Technology, Ningbo, China. Her research interests include intelligent optimization, modeling and its applications to electronic system design and control

system design.



Huiyu Zhou received a Bachelor of Engineering degree in Radio Technology from Huazhong University of Science and Technology of China, and a Master of Science degree in Biomedical Engineering from University of Dundee of United Kingdom, respectively. He was awarded a Doctor of Philosophy degree in Computer Vision from Heriot-Watt University, Edinburgh, United Kingdom. Dr. Zhou currently is a Reader at Department of Informatics, University of Leicester, United Kingdom. He has published over 150 peer-reviewed papers in the field.

His research work has been or is being supported by UK EPSRC, MRC, EU, Royal Society, Leverhulme Trust, Puffin Trust, Invest NI and industry.